Plasma transport in a converging magnetic field with applications to helicon plasma thrusters

IEPC-2013-125

Justin M. Little[*] and Edgar Y. Choueiri[†]
Princeton University, Princeton, New Jersey, 08540, USA

Plasma transport in the convergent magnetic field region of an RF plasma source with a movable rear gas injection wall is investigated using an RF compensated Langmuir probe to support the development of helicon plasma thrusters. Measurements of the radial plasma density profile show that the plasma structure consists of convective and diffusive regions. The width of the convective region is shown to scale according to the bounding magnetic flux surface that intersects the gas injection plane. The extent of the diffusive region is governed by a parameter, τ, which is the ratio of the convective to diffusive timescales. The plasma is observed to transition to a convective mode for $\tau < 0.1$, which represents a new design criteria for helicon plasma thrusters.

I. Introduction

Electrodeless acceleration of plasma generated by radio-frequency (RF) waves may provide the foundation for a new class of high-efficiency, long-lifetime electric propulsion systems. In its electrothermal form, plasma formed through the absorption of RF power into a propellant gas is channeled through a convergent-divergent magnetic field, or magnetic nozzle (MN).[1,2] Depending on the system, ion acceleration is achieved through one or a combination of the following phenomena: ion magnetic moment conservation,[3,4] ambipolar electric fields resulting from electron thermal expansion,[5–7] and current-free double-layers.[8–10] Momentum is transferred back to the MN by internal plasma currents.[11,12]

One such device is the helicon plasma thruster (HPT),[13–17] which is the commonly used nomenclature when low-frequency (typically 13.56 MHz) RF waves are used with plasma source geometries that favor the propagation of helicon waves. Early in its development, thrust measurements with the HPT have yielded poor performance.[15–19] Consistent with previous helicon sources, many of these concepts used uniform magnetic fields within the plasma source. Improved performance was observed by Takahashi[15,20] for an applied magnetic field that approximated a dipole-like field with the peak magnitude at the exit of the thruster. That configuration has the best measured performance to date, with 15 mN of thrust, $2,000$ s specific impulse, and 7.5% thrust efficiency.

Varying levels of performance have been measured for different magnetic and physical HPT geometries, however, the specific processes that underly this performance variation have not been investigated in detail. The goal of this paper is to experimentally investigate the dominant plasma transport mechanisms within the HPT source region, and use this understanding to answer the following questions: How does the plasma profile along the magnetic nozzle depend on the magnetic and physical geometries of the plasma source? How do these geometries influence the predicted HPT performance?

We will experimentally investigate the plasma transport mechanisms in an HPT using Langmuir probe measurements of the plasma for various magnetic field strengths and plasma source lengths. We provide a detailed description of the plasma source and Langmuir probe in Sec. II. Sec. III contains a description of

---

[*]Graduate Research Assistant, Mechanical and Aerospace Engineering, jml@princeton.edu.
[†]Chief Scientist, EPPDyL; Professor, Applied Physics Group, Mechanical and Aerospace Engineering.
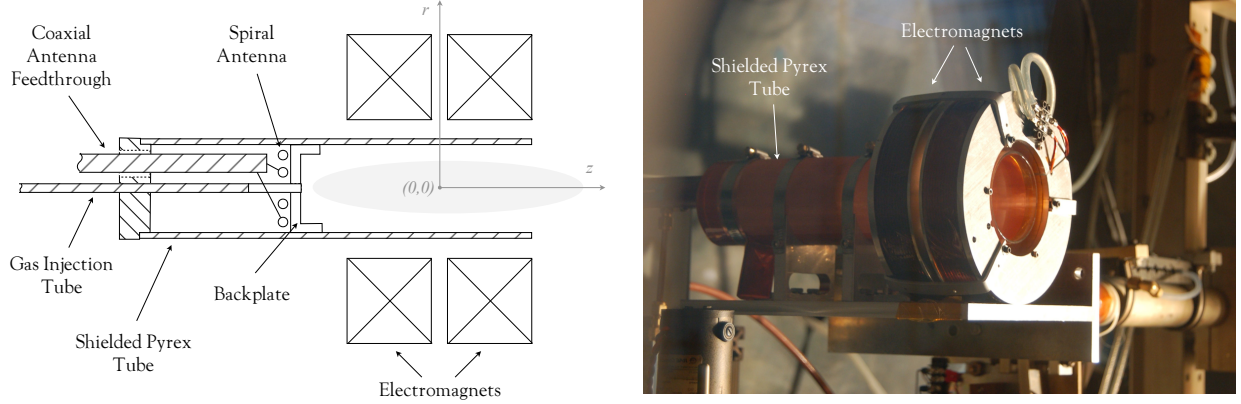
Figure 1. Schematic (left) and picture (right) of the flat-spiral antenna RF plasma source.

two different operation modes that we observed in the plasma, Langmuir probe measurements of the plasma density and temperature, and an analysis of the plasma transport based on the radial density profile of the plasma.

II.   Experimental Setup

We investigate plasma transport in an HPT using a flat-spiral antenna RF plasma testbed that we designed and constructed to allow for quick adjustment of the physical and magnetic geometries of the plasma source. We measure the radial profile of the electron temperature and density at the point of maximum magnetic field, or MN throat, using an RF compensated Langmuir probe for various magnetic field strengths and gas injection locations. From these measurements we draw conclusions about the dominant plasma transport mechanisms within the device.
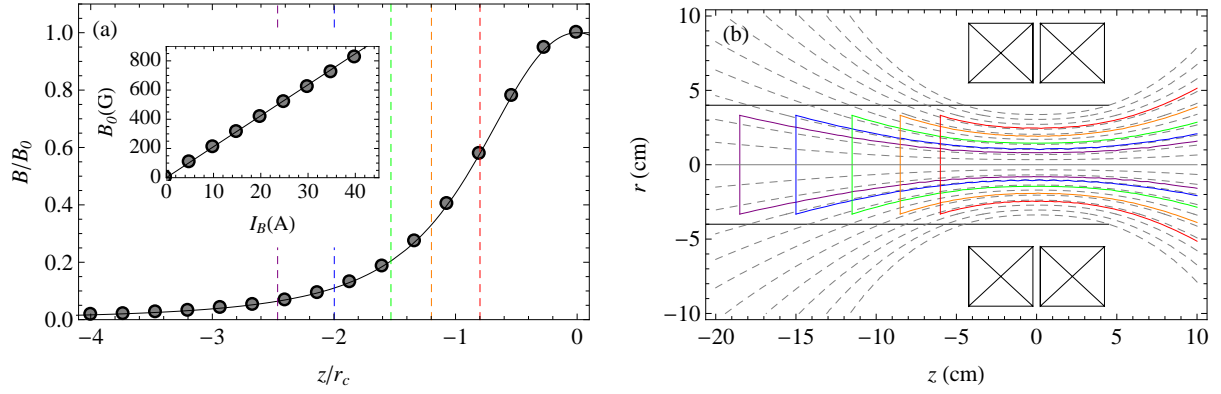
A.   Plasma Source

The plasma source (PS) (Fig. 1) consists of an 8.0 cm diameter, 30.5 cm long tube of borosillicate glass mounted concentrically inside two electromagnetic coils. The tube is wrapped with copper mesh to prevent stray RF fields outside of the PS. The entire assembly is mounted on a flat plate that is attached to the end of a swinging-arm thrust stand, which will not be used in this study.

We use a two-turn spiral antenna positioned within the glass tube to excite the plasma. The antenna is not mechanically connected to either the PS or any components on the thrust stand. Using an alumina injection tube, gas is fed through the center of a Macor backplate, which is used to isolate the plasma from the antenna. We designed the matching network such that the antenna leads are mounted on two copper rail electrodes that are aligned parallel to the axis of the device to allow adjustment of the axial position of the antenna. Furthermore, the Macor backplate and gas injection tube may be translated axially to remain next to the antenna. This design allows for adjustment of the axial position of the antenna and gas injection location within a 13 cm range.

The RF signal is produced using an Agilent 8648B signal generator. An ENI 2100L pre-amplifier steps the signal up to approximately 20 W, which is fed into a Alpha 9500 linear amplifier capable of producing 1.5 kW. An Alpha 4520 digital wattmeter is used to monitor the standing-wave ratio (SWR) and determine the power delivered to the matching network/antenna (P_D). This system is capable of generating RF power over a range of frequencies, however, we limit our tests to 13.56 MHz.

The power is transferred to the antenna via an L-type impedance matching network mounted rigidly inside of the vacuum chamber (isolated mechanically from the thrust stand). The matching network consists of two Comet vacuum-variable capacitors with a range of $5 - 500$ pF. Each capacitor is rated at 5kV. Depending on the antenna position, the experiment was performed with SWR's between 1.0 and 2.5, with

2

The 33rd International Electric Propulsion Conference, The George Washington University, USA
October 6–10, 2013

Figure 2. Magnetic field configuration. (a) Axial variation of the magnetic field strength, B, relative to it's value at the throat, B_0. The insert shows the dependence of B_0 on the magnet current, I_B. The colored dashed lines indicate the different injection locations used throughout the experiment. (b) Magnetic flux contours (dashed) are shown along with the flux contours corresponding to the plane of the various injection locations.

larger SWRs observed for a longer effective antenna length. Frequency adjustments on the order of 0.01 MHz were sometimes used to obtain a better match.[21]

The electromagnets were made by wrapping 144 turns (12×12) of AWG 10 square, copper magnet wire wound around an aluminum mandrel. The effective radius of each coil was measured to be $r_c = 7.51$ cm, which corresponds closely to the physical radius of the center of the copper windings. The magnets are powered using an Amrel SPS32 DC switching power supply, and are each capable of handling up to 50 A of current.

The magnets were designed such that they may move independently with respect to each other and the glass tube, thus allowing control over the physical and magnetic geometries of the PS. A single configuration is used throughout the duration of this experiment (Fig. 1) whereby the magnets are connected rigidly together with an axial separation of 4.5 cm. The surface of the magnet furthest downstream from the antenna is aligned with the end of the glass tube.

Measurements of the relative magnetic field strength along the nozzle axis are shown in Fig. 2(a). The magnitude of the maximum magnetic field as a function of the coil current, I_B, is also shown in the insert. The solid black lines in Fig. 2(a) result from approximating the two magnets as single loops of current with radius r_c. Continuing with this approximation, the surfaces of constant magnetic flux are shown in Fig. 2(b) as dashed lines. The colored lines correspond to the different injection planes and bounding magnetic flux surfaces used throughout the experiment.

All of the experiments are performed within the EPPDyL's Large Dielectric Pulsed Propulsion (LDPP) vacuum chamber. The cylindrical chamber is made out of fiberglass and measures 8 ft. in diameter and 25 ft. in length. The chamber is evacuated using two mechanical Stokes roughing pumps, a roots blower, and a 48 inch diameter CVC diffusion pump rated at 95,000 l/s of pumping capacity. The facility is also equipped with liquid nitrogen baffles, which are not used in this experiment. Pressure is measured using a Varian ConvectTorr vacuum gauge and Varian 525 cold cathode gauge connected to a Varian L8350 multi-gauge controller. The vacuum system is capable of achieving base pressures of 2×10^{-6} Torr, however, vacuum leaks restricted the base pressure of the present experiments to 5×10^{-5} Torr.

The experiment was operated in steady-state for typical durations of two hours, during which the chamber pressure never exceeded 1×10^{-4} Torr. Temperatures were monitored using a Flir i7 infrared camera to prevent overheating. "Hot spots" were observed at gas injection location and the matching network. Following two hours of operation, the system was allowed to cool down to nominal temperatures. Significant heating of the magnets occurred for extended operation with $I_B > 30$ A. Because the magnets are passively cooled, the system required overnight rest if the magnets exceeded a threshold temperature.

B. Diagnostics

The primary diagnostic used in this study is an RF compensated Langmuir probe (LP).[22] The probe tip is made of tungsten wire and has a 0.25 mm diameter and 1.0 mm length. The wire is friction-fit to a stainless steel tube and inserted in an alumina tube. A 0.1 mm wide by 0.5 mm deep recess exists between the probe tip and alumina jacket so that the tip remains electrically isolated from any conductive coating that could potentially be sputtered onto the jacket. Partial RF compensation is achieved using four self-resonant chip inductors: two each with a resonant frequency of 14 MHz and 28 MHz. The inductors are soldered between the stainless steel tube and shielded steel wire that leads to a BNC termination. The compensation circuit and steel wire are housed in a 1/4" diameter by 12" long alumina tube, which is connected on opposite ends to the smaller alumina tube and a BNC termination using Torr Seal.

The LP is mounted on a small fiberglass rod positioned perpendicular to the thruster axis and located approximately 30 cm from the exit of the plasma source. The axial location of the LP corresponds to the location of maximum applied magnetic field ($z = 0$), while the radial location is controlled with a single-axis translation stage.

The LP bias voltage is produced by a three-stage phase shift oscillator that drives a Kepco 1000M bi-polar operational power/amplifier (BOP) to produce a 5 Hz, 140V peak-to-peak waveform. The BOP is connected to the LP using BNC cables on each side of a vacuum feedthrough. Current from (to) the probe is measured across the 1 kΩ resistor of a low-pass filter and displayed on a Tektronix TDS 3034B digital oscilloscope.

Typical current-voltage (IV) curves are obtained by averaging over eight waveform periods. The electron temperature is found from the inverse of the slope of the linear region of the ln I-V graph. The error due to this method for our LP is estimated as 25%. It is possible to decrease this error using an additional electrode to act as a reference for the plasma potential,[22] however, this occurs at the cost of added complexity and intrusiveness.

The plasma density, n_i, was found from the ion saturation region of the IV curve. Sheath expansion effects of cylindrical LPs have previously been accounted for in the literature by linear extrapolation of the ion saturation current to either the floating potential, V_f, or the plasma potential V_p.[23,24] We obtain n_i from the average of these two methods, and estimate the error as one-half of the difference between these methods added in quadrature with the influence of uncertainty in the electron temperature.

III.   Plasma Characterization

We investigate the transport of plasma through the PS by taking radial LP measurements at the point of maximum magnetic field, or throat. Unless otherwise specified, measurements are taken at a fixed delivered power, $P_D = 500$ W, and argon mass flow rate, $\dot{m}_{Ar} = 2$ mg/s. We take data for five different axial locations of the Macor injection backplate, which will correspond to the following magnetic flux contour colors in Fig. 2: $z_{\rm bp} = -6.0$ cm (Red), $z_{\rm bp} = -8.5$ cm (Orange), $z_{\rm bp} = -11.5$ cm (Green), $z_{\rm bp} = -15.0$ cm (Blue), and $z_{\rm bp} = -18.0$ cm (Purple). The radius of the Macor injection region is 3.1 cm.

A.   Low-Field Mode Transition

The plasma source was observed to operate in two distinct modes depending on the argon mass flow rate, applied magnetic field strength, injection location, and RF power. In general, the discharge with low magnetic fields at the injection plane appeared much brighter than the mode that occurred at higher magnetic fields. Because we do not characterize each mode in depth, we refer to the low-magnetic field mode simply as the high-energy (HE) mode, and the high-magnetic field mode as the low-energy (LE) mode. This distinction will soon become apparent.

The dependence of the electron temperature and plasma density on the magnet current is shown in Fig. 3 for $P_D = 500$ W, $\dot{m}_{Ar} = 2$ mg/s, and $z_{\rm bp} = -11.5$ cm. In the HE mode, it is clear that the plasma density at the throat increases with the applied magnetic field until it reaches an asymptote of around 3×10^{18} m^{-3}. As the magnetic field is increased beyond a certain threshold ($I_B \approx 26$ A in Fig. 3), the plasma falls back to the LE mode, which is characterized by densities on the order of 10^{16} m^{-3} and remains stable for higher magnetic fields (not shown in the data). The arrows in Fig. 3(a) depict the hysteresis associated with the mode transition, which was also observed in a spiral antenna RF plasma source by Lho *et al.*[25]

The LE mode is observed to have a higher electron temperature ($T_e \sim 10$ eV) than the HE mode ($T_e \sim 7$ eV). Furthermore, the electron temperature of the HE mode appears to increase with I_B, however, the
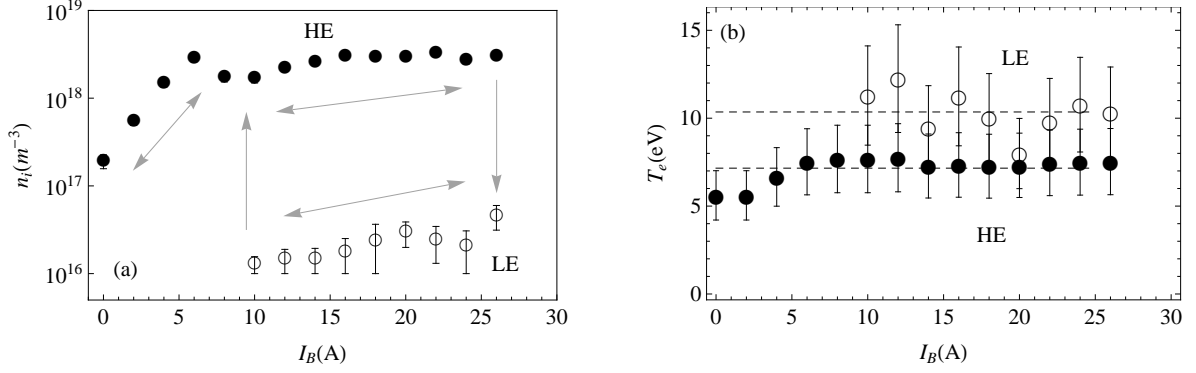
4

The 33rd International Electric Propulsion Conference, The George Washington University, USA
October 6–10, 2013

Figure 3. Plasma mode transition. (a) LP measurements of the plasma density, n_i, as a function of the magnet current, I_B for the high-energy (HE) and low-energy (LE) modes. (b) LP measurements of the electron temperature, T_e, as a function of the magnet current, I_B.
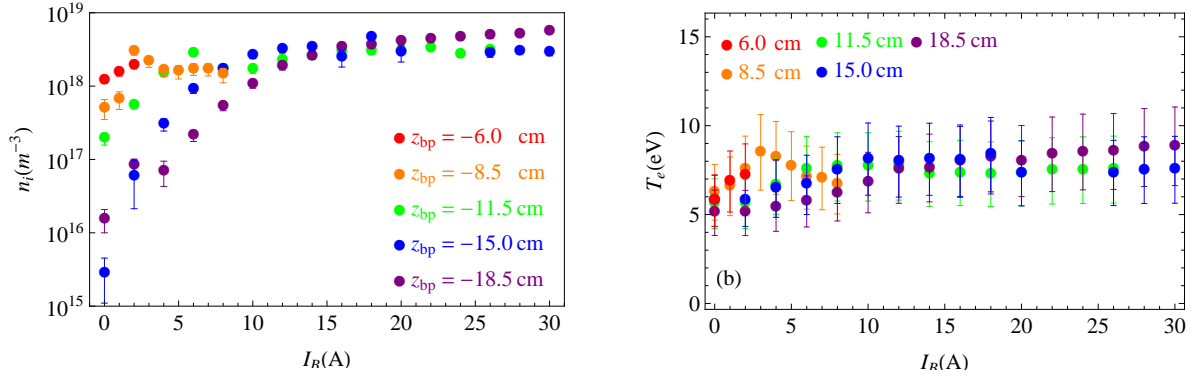

Figure 4. LP Data for the HE mode. (a) Plasma density, n_i, and (b) electron temperature, T_e, as a function of magnet current, I_B, for various injection locations, z_{bp}.
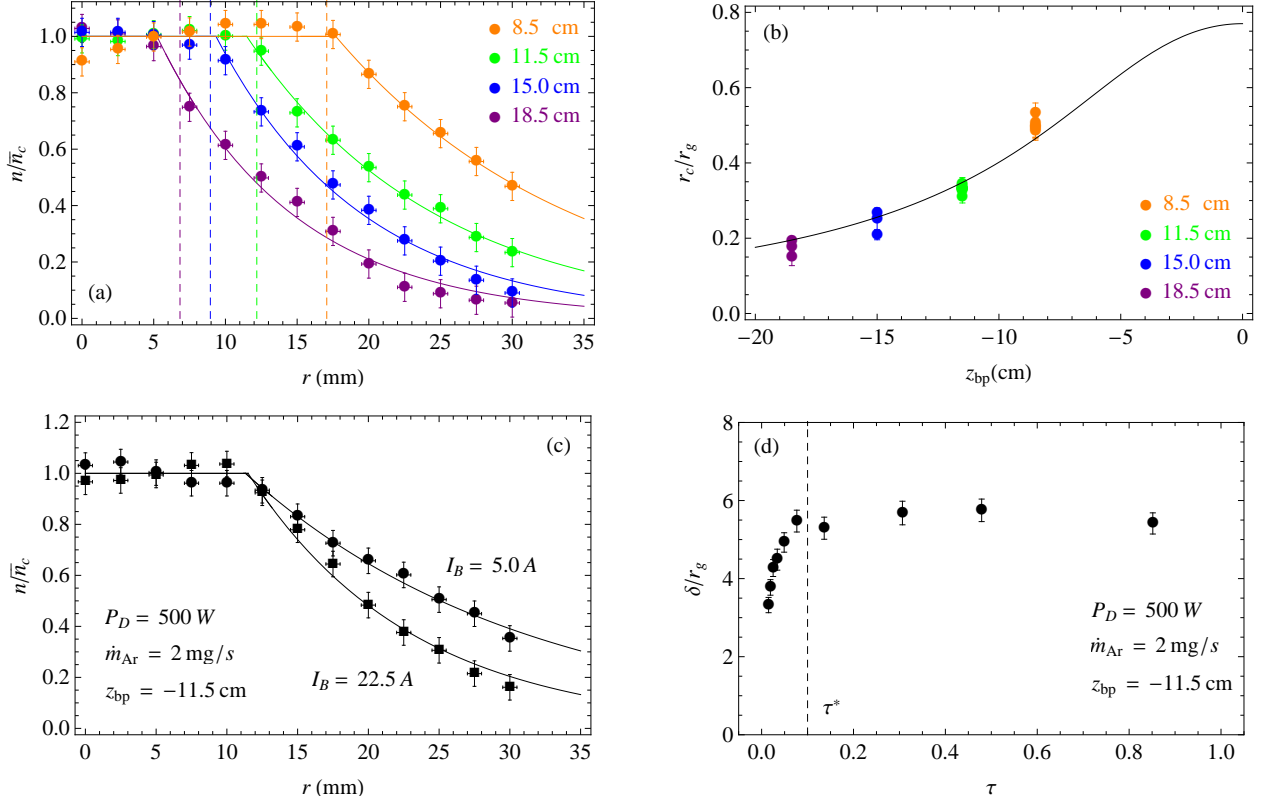
increase is on the order of the experimental uncertainty of the LP.

Helicon modes in low-magnetic field RF plasmas have previously been observed in the literature,[26, 27] and have been recently studied in depth by Lafleur *et al.*[28–31] A few curious distinctions between the mode transitions observed in our PS (using a spiral antenna) and those found in literature (typically with a Boswell-type antenna) are worth mention: (1) the HE mode in our experiment is stable at zero applied magnetic field, which was also observed by Lho *et al.*;[25] (2) the HE mode exists for applied magnetic fields an order of magnitude larger than previously observed; and, (3) the density jumps by around two orders of magnitude between the two modes, as compared to less than an order of magnitude observed in the literature. These distinctions will be the topic of a future study.

B.   Density and Temperature Measurements

The data presented throughout the rest of the paper will be focused on the HE mode, as its high densities imply high ionization fractions, which are of interest for plasma propulsion applications. In this section we present density measurements as a function of the magnet current for various gas injection locations. The LP was positioned at the center of the magnets along the throat plane: $(r, z) = (0, 0)$.

A similar trend is seen in Fig. 4(a) for n_i vs. I_B for different values of z_{bp}. Specifically, the plasma density increases with the applied magnetic field towards an asymptotic value. It was observed that this asymptotic value increased with both $\dot{m}_{\mathrm{Ar}}$ and P_D, implying that the peak density at high magnetic fields is determined

5

The 33rd International Electric Propulsion Conference, The George Washington University, USA
October 6–10, 2013

Figure 5. Plasma transport. (a) Radial density LP measurements for various injection planes (circles) compared to the model (solid lines) of Eq. (1) with r_c and δ found from the method of least-squares. Dashed lines correspond to the location of r_c predicted from Eq. (2). **(b)** Measured (circles) and predicted (line) values of r_c versus the back plate location, z_{bp}. **(c)** Radial density LP measurements for two different magnet currents. **(d)** Measured diffusion length scale, δ, versus the parameter τ, which is the ratio of the convective to diffusive timescales of the plasma. A distinct transition occurs near $\tau^* \approx 1$.

mainly by the availability of gas atoms in this region and the amount of power for ionization.

The plasma density as $I_B \to 0$ decreases drastically (over nearly three orders of magnitude) as the distance between the injection plane and throat increases. This is a result of plasma absorption at the walls of the glass tube as the radial diffusion of the plasma increases as the magnetic field decreases. In fact, measurements using an infrared camera indicated increased heating of the glass tube for low magnetic fields. Furthermore, the area over which the plasma is absorbed increases as $|z_{bp}|$ increases. The relation between the cross-field diffusion of the plasma and convection along the magnetic field lines is investigated in further detail in Sec. C.

Finally, we note that the electron temperature showed a slight increase with the magnet current for each injection location, however, this increase was within the experimental uncertainties. Furthermore, the electron temperature remained around 7 eV.

C. Radial Plasma Structure and Transport Mechanisms

LP measurements showing the radial dependence of the plasma density at $z = 0$ is shown in Fig. 5(a) for various z_{bp}. Here, the densities are normalized by $\bar{n}_c$, which will be defined later. In general, the plasma density remains uniform near the axis of the PS to a certain radial distance, after which the density falls off exponentially.

Based on the radial density measurements, we propose the following physical picture to describe the structure of the plasma within the source region. Plasma formed in the injection region ($z = z_{bp}$) with a radially uniform density profile convects along the converging magnetic field towards the throat plane ($z = 0$). The density profile at the throat will remain uniform in the limit that transport is governed purely

6

The 33rd International Electric Propulsion Conference, The George Washington University, USA
October 6–10, 2013

by convection. However, the plasma density spreads out radially due to ambipolar cross-field diffusion (either collisional or collisionless). The radial uniformity of the density profile in the injection region is inferred from the fact that the density profile for $I_B = 0$ is highly uniform, and becomes even more uniform as $|z_{bp}|$ decreases. Furthermore, the exponential radial dependence of the plasma density in the diffuse region is predicted from the diffusion equation.[32]

Using this physical picture, we propose the following model to describe the plasma density profile at the throat of the PS:

$$n_i(r) = \begin{cases} \bar{n}_c & : r < r_c \\ \bar{n}_c \exp\left[-\left(r - r_c\right)/\delta\right] & : r > r_c \end{cases} \tag{1}$$

Here, r_c defines the boundary between the convective ($r < r_c$) and diffusive ($r > r_c$) regions of the plasma, $\bar{n}_c$ is the average plasma density in the convective region, and δ is the diffusion length scale. The solid lines in Fig. 5(a) are the result of a least-squares fit of Eq. (1) to the LP data.

It is clear from Fig. 5 that r_c increases as $|z_{bp}|$ decreases. For convection along a magnetic field, the radius of the plasma is predicted to scale according to

$$r_c \approx r_i \sqrt{\frac{B_i}{B}}, \tag{2}$$

where we have assumed $B_z \gg B_r$. Here, r_i is the radius of the injection region and B_i is the magnitude of the magnetic field at the injection plane. Fig. 5(b) compares the measured values of r_c compared the values predicted by Eq. (2). Here, r_c is normalized by the radius of the glass tube, r_g. The good agreement between the calculated and predicted values of r_c supports the physical notion that the uniform portion of the plasma is convected, or channeled, along the magnetic field lines.

We now turn our attention to the diffusive region of the plasma. As shown in Fig. 5(c), the radial density profile in the diffusive region of the plasma steepens as the applied magnetic field increases, which corresponds to a decrease in δ. This is physically intuitive because one would expect the cross-field transport of the plasma to decrease with increasing field strength.

The relative importance of plasma convection to plasma diffusion may be analyzed using the parameter,

$$\tau \equiv \frac{t_c}{t_d} = \frac{L_c D_\perp}{c_s r_g^2}, \tag{3}$$

which is defined as the ratio of the convective timescale, $t_c = c_s/L_c$, to the diffusive timescale, $t_d = r_g^2/D_\perp$, of the plasma. Here, $L_c = |z_{bp}|$ is the effective chamber length, $c_s = (k_b T_e/m_i)^{1/2}$ is the ion acoustic velocity, $D_\perp$ is the cross-field diffusion coefficient, and r_g is the radius of the confining physical boundary (the glass tube in our experiment).

We take $D_\perp$ to be the classical cross-field diffusion coefficient for a fully ionized gas, which may be approximated as[32]

$$D_\perp \approx 1.67 \times 10^{-14} \frac{n_i}{T_e^{1/2} B^2} \quad \left[m^2/s\right]. \tag{4}$$

Here, n_i, T_e, and B are given in units of m^{-3}, eV, and G, respectively.

The experimentally measured quantity δ/r_g is plotted in Fig. 5(d) against τ for $P_D = 500$ W, $\dot{m}_{Ar} = 2$ mg/s, and $z_{bp} = -11.5$ cm. Here, τ is calculated using the magnitude of the magnetic field at the injection plane, B_i, and assuming $n_i = 10^{18}$ m^{-3} and $T_e = 7 eV$. Thus, increasing τ corresponds to decreasing B_i.

A clear transition is observed around $\tau = \tau^* \approx 0.1$. For $\tau \ll \tau^*$, δ trends towards zero with decreasing τ, which indicates that the flow is primarily channeled through the applied magnetic field and is in a convective regime. In the limit where $\tau \gg \tau^*$, δ approaches a constant value with respect to τ. This limit is characterized by very low magnetic fields, thus implying that the plasma has become de-magnetized and is in a fully diffusive regime. Finally, $\tau \approx \tau^*$ is characteristic of a transition regime in which both convection along the field lines and cross-field diffusion govern the plasma profile at the throat plane.

IV. Conclusions

We are now in the position to answer the question posed at the outset: *how do the magnetic and physical geometries influence of a helicon plasma thruster influence its propulsive performance?* Using LP

7

The 33rd International Electric Propulsion Conference, The George Washington University, USA
October 6–10, 2013

measurements of the radial plasma density profile for different gas injection locations with respect to the applied magnetic field maximum, we demonstrated that the flow into the magnetic nozzle region of the thruster is governed by a balance between convective and diffusive transport.

In the convective regime ($\tau \ll \tau^*$), the converging magnetic field configuration, observed by Takahashi et al. to be superior to the uniform magnetic field configuration,[15, 20] leverages convective transport along the magnetic field lines to keep the bulk of the plasma from impinging on the side walls of the thruster. The plasma at the magnetic nozzle throat becomes more focused towards the axis as the injection plane is pushed further upstream, which is predicted to improve the divergence efficiency of the exhaust.[11, 33] A tradeoff exists, however, as pushing the injection plane upstream increases both L_c and $D_\perp$ in Eq. (3). Therefore, the applied magnetic field must increase according to $B_0 \sim L_c^2/\tau^{1/2}$. Recent results by Takahashi et al.[34] suggest that increasing the magnitude of the magnetic field improves performance by also limiting the cross-field diffusion of the plasma in the expansion region of the MN.

The downside of the converging magnetic field configuration is that nothing prevents the plasma from impacting the backplate of the thruster. Indeed, significant heating of the backplate was observed throughout our experiments, which was predicted theoretically by Ahedo and Navarro-Cavallé.[35] A magnetic mirror configuration may be capable of limiting the power losses to the back wall of the plasma source.[36] The implications of the mirror field on the plasma transport are beyond the scope of this paper, and will be left for future research.

Acknowledgments

References

[1] Andersen, A., Jensen, V., Nielsen, P., and D'Angelo, N., "Continuous supersonic plasma wind tunnel," Physics Letters A, Vol. 27, No. 8, 1968, pp. 527–528.

[2] Kuriki, K. and Okada, O., "Experimental Study of a Plasma Flow in a Magnetic Nozzle," Physics of Fluids, Vol. 13, 1970, pp. 2262.

[3] Comfort, R., "The magnetic mirror force in plasma fluid models," Modeling magnetospheric plasma, 1988, pp. 51–53.

[4] Longmier, B. W., Cassady, L. D., Ballenger, M. G., Carter, M. D., Chang-Díaz, F. R., Glover, T. W., Ilin, A. V., McCaskill, G. E., Olsen, C. S., Squire, J. P., et al., "VX-200 magnetoplasma thruster performance results exceeding fifty-percent thruster efficiency," Journal of Propulsion and Power, Vol. 27, No. 4, 2011, pp. 915–920.

[5] Arefiev, A. V. and Breizman, B. N., "Ambipolar acceleration of ions in a magnetic nozzle," Physics of Plasmas, Vol. 15, No. 4, 2008, pp. 042109.

[6] Longmier, B., Bering, E., Carter, M., and Others, "Ambipolar ion acceleration in an expanding magnetic nozzle," Plasma Sources Science and Technology, Vol. 20, 2011, pp. 015007.

[7] Charles, C., Boswell, R., and Takahashi, K., "Boltzmann expansion in a radiofrequency conical helicon thruster operating in xenon and argon," Applied Physics Letters, Vol. 102, 2013, pp. 223510.

[8] Charles, C. and Boswell, R., "Current-free double-layer formation in a high-density helicon discharge," Applied Physics Letters, Vol. 82, No. 9, 2003, pp. 1356.

[9] Fruchtman, A., "Electric field in a double layer and the imparted momentum," Physical review letters, Vol. 96, No. 6, 2006, pp. 065002.

[10] Ahedo, E., "Double-layer formation and propulsive assessment for a three-species plasma expanding in a magnetic nozzle," Physics of Plasmas, Vol. 18, No. 3, 2011, pp. 033510.

[11] Ahedo, E. and Merino, M., "Two-dimensional supersonic plasma acceleration in a magnetic nozzle," Physics of Plasmas, Vol. 17, No. 1, 2010, pp. 1–16.

[12] Takahashi, K., Lafleur, T., Charles, C., Alexander, P., and Boswell, R., "Electron Diamagnetic Effect on Axial Force in an Expanding Plasma: Experiments and Theory," Physical Review Letters, Vol. 107, No. 23, Nov. 2011, pp. 1–4.

[13] Winglee, R., Ziemba, T., Giersch, L., Prager, J., Carscadden, J., and Roberson, B. R., "Simulation and laboratory validation of magnetic nozzle effects for the high power helicon thruster," Physics of Plasmas, Vol. 14, No. 6, 2007, pp. 063501.

[14] Batishchev, O. V., "Minihelicon Plasma Thruster," IEEE Transactions on Plasma Science, Vol. 37, No. 8, Aug. 2009, pp. 1563–1571.

[15] Takahashi, K., Lafleur, T., Charles, C., Alexander, P., Boswell, R. W., Perren, M., Laine, R., Pottinger, S., Lappas, V., Harle, T., and Lamprou, D., "Direct thrust measurement of a permanent magnet helicon double layer thruster," Applied Physics Letters, Vol. 98, No. 14, 2011, pp. 141503.

[16] Williams, L. T. and Walker, M. L., "Thrust Measurements of a Radio Frequency Plasma Source," Journal of Propulsion and Power, Vol. 29, No. 3, 2013, pp. 520–527.

[17] Shabshelowitz, A. and Gallimore, A. D., "Performance and Probe Measurements of a Radio-Frequency Plasma Thruster," Journal of Propulsion and Power, 2013, pp. 1–11.

[18]Ling, J., West, M., Lafleur, T., Charles, C., and Boswell, R., "Thrust measurements in a low-magnetic field high-density mode in the helicon double layer thruster," Journal of Physics D: Applied Physics, Vol. 43, No. 30, 2010, pp. 305203.

[19]Pottinger, S., Lappas, V., Charles, C., and Boswell, R., "Performance characterization of a helicon double layer thruster using direct thrust measurements," Journal of Physics D: Applied Physics, Vol. 44, No. 23, 2011, pp. 235201.

[20]Takahashi, K., Charles, C., Boswell, R., and Ando, A., "Performance improvement of a permanent magnet helicon plasma thruster," Journal of Physics D: Applied Physics, Vol. 46, No. 35, 2013, pp. 352001.

[21]Charles, C., Boswell, R., and Bish, A., "Variable frequency matching to a radiofrequency source immersed in vacuum," Journal of Physics D: Applied Physics, Vol. 46, No. 36, 2013, pp. 365203.

[22]Sudit, I. D. and Chen, F. F., "RF compensated probes for high-density discharges," Plasma Sources Science and Technology, Vol. 3, No. 2, 1994, pp. 162.

[23]Chen, F. F., "Langmuir probe analysis for high density plasmas," Physics of Plasmas, Vol. 8, 2001, pp. 3029.

[24]Smirnov, A., Raitses, Y., and Fisch, N., "Plasma measurements in a 100 W cylindrical Hall thruster," Journal of Applied Physics, Vol. 95, No. 5, 2004, pp. 2283–2292.

[25]Lho, T., Hershkowitz, N., Miller, J., Steer, W., and Kim, G.-H., "Azimuthally symmetric pseudosurface and helicon wave propagation in an inductively coupled plasma at low magnetic field," Physics of Plasmas, Vol. 5, 1998, pp. 3135.

[26]Stevens, J., Sowa, M., and Cecchi, J., "Helicon plasma source excited by a flat spiral coil," Journal of Vacuum Science & Technology A: Vacuum, Surfaces, and Films, Vol. 13, No. 5, 1995, pp. 2476–2482.

[27]Sato, G., Oohara, W., and Hatakeyama, R., "Experimental characterization of a density peak at low magnetic fields in a helicon plasma source," Plasma Sources Science and Technology, Vol. 16, No. 4, 2007, pp. 734.

[28]Lafleur, T., Charles, C., and Boswell, R., "Ion beam formation in a very low magnetic field expanding helicon discharge," Physics of Plasmas, Vol. 17, 2010, pp. 043505.

[29]Lafleur, T., Charles, C., and Boswell, R., "Plasma control by modification of helicon wave propagation in low magnetic fields," Physics of Plasmas, Vol. 17, 2010, pp. 073508.

[30]Lafleur, T., Charles, C., and Boswell, R., "Characterization of a helicon plasma source in low diverging magnetic fields," Journal of Physics D: Applied Physics, Vol. 44, No. 5, 2011, pp. 055202.

[31]Lafleur, T., Charles, C., and Boswell, R., "Electron–cyclotron damping of helicon waves in low diverging magnetic fields," Physics of Plasmas, Vol. 18, 2011, pp. 043502.

[32]Chen, F. F., Introduction to plasma physics and controlled fusion. Volume 1, Plasma physics, Springer, 2nd ed., 1984.

[33]Little, J. M. and Choueiri, E. Y., "Thrust and Efficiency Model for Electron-Driven Magnetic Nozzles," Physics of Plasmas, 2013, (In Press).

[34]Takahashi, K., Charles, C., and Boswell, R. W., "Approaching the Theoretical Limit of Diamagnetic-Induced Momentum in a Rapidly Diverging Magnetic Nozzle," Physical review letters, Vol. 110, No. 19, 2013, pp. 195003.

[35]Ahedo, E. and Navarro-Cavallé, J., "Helicon thruster plasma modeling: Two-dimensional fluid-dynamics and propulsive performances," Physics of Plasmas, Vol. 20, 2013, pp. 043512.

[36]Cohen, S. A., Siefert, N., Stange, S., Boivin, R., Scime, E., and Levinton, F., "Ion acceleration in plasmas emerging from a helicon-heated magnetic-mirror device," Physics of Plasmas, Vol. 10, 2003, pp. 2593.